FRONTIERS OF PHYSICS

RESEARCH ARTICLE
Volume 18 / Issue 6 / 62303 / 2023

Realization of highly isolated stable few-spin systems based on alkaline-earth fermions

Wen-Wei Wang[1,2,*], Han Zhang[1,2,*,†], Chang Qiao[1,2], Ming-Cheng Liang[1,2,3], Rui Wu[1,2], Xibo Zhang[1,2,3,4,‡]

1 International Center for Quantum Materials, School of Physics, Peking University, Beijing 100871, China
2 Collaborative Innovation Center of Quantum Matter, Beijing 100871, China
3 Beijing Academy of Quantum Information Sciences, Beijing 100193, China
4 Hefei National Laboratory, Hefei 230088, China
*These authors contributed equally to this work.
Corresponding authors. E-mail: †han.z@pku.edu.cn, ‡xibo@pku.edu.cn
Received March 16, 2023; accepted May 30, 2023

ABSTRACT

Few-level systems consisting of a certain number of spin states have provided the basis of a wide range of cold atom researches. However, more developments are still needed for better preparation of isolated few-spin systems. In this work, we demonstrate a highly nonlinear spin-discriminating (HNSD) method for isolating an arbitrary few-level manifold out of a larger total number of spin ground states in fermionic alkaline-earth atoms. With this method, we realize large and tunable energy shifts for unwanted spin states while inducing negligible shifts for the spin states of interest, which leads to a highly isolated few-spin system under minimal perturbation. Furthermore, the isolated few-spin system exhibits a long lifetime on the hundred-millisecond scale. Using the HNSD method, we demonstrate a characteristic Rabi oscillation between the two states of an isolated two-spin Fermi gas. Our method has wide applicability for realizing long-lived two-spin or high-spin quantum systems based on alkaline-earth fermions.

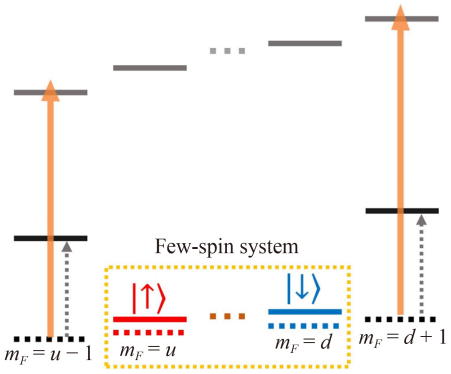

Keywords few-spin system, alkaline-earth atoms, ultracold Fermi gas, a.c. Stark shift, long-lived quantum system

1 Introduction

The realization of few-spin systems plays an important role in numerous cold atom studies, providing a basic ingredient in research fields including precision frequency metrology [1], few-body interaction physics [2, 3], programmable quantum simulations of spin systems [4], and quantum simulation of topological models [5–9]. In these researches, the performance of multi-spin quantum materials can be influenced by a fundamental issue, namely how well an energetically stable few-spin system can be prepared and isolated from the rest of spin ground states. In the field of ultracold atoms, few-spin manifolds of alkali metal atoms have been prepared by applying a sufficiently large magnetic field that induces nonlinear Zeeman energy shifts with respect to the magnetic quantum number (via the second-order Zeeman effect) [8–10]. In this approach, it can require sophisticated magnetic field control with 10^{-5} G stability [10, 11] to achieve long lifetime of the system, which is very challenging to implement for fermionic isotopes such as ^{6}Li and ^{40}K that in general operate at relatively

Higher Education Press

https://doi.org/10.1007/s11467-023-1314-2

large fields of hundreds of Gausses.

In contrast to alkali metal atoms, alkaline-earth atoms (AEAs) have unique properties that enable different routes for the realization of few-spin systems [1, 12–33]. First, AEA spin ground states are highly insensitive to an external magnetic field [14], whereas the spin excited states remain sensitive to the field. Second, AEAs have an inter-combination transition with a very narrow linewidth in the kHz range. These properties together make it possible to develop optical approaches for individually addressing chosen AEA spin ground states in the frequency space based on the narrow-linewidth transition, which has the potential to realize a manifold of an arbitrary number of spin states and to engineer such spin configuration with high spatial resolution and fast modulation speed.

A number of progresses have been made for manipulating AEA spin ground states. In the absence of near-resonant inter-spin couplings, various initial spin configurations can be prepared by single- or multi-stage optical pumping and manipulation methods [1, 15–20] or by spin distillation technique without optical excitation [31], which are further protected by the suppression of spin-changing collisions due to the $SU(\mathcal{N})$-symmetric nature of AEAs in the $^1S_0$ ground state. Furthermore, when near-resonant inter-spin couplings such as spin–orbit couplings [34–37] are realized as a key feature in a quantum system of AEAs, a much more stringent requirement is raised for realizing a few-spin manifold that is not only energetically stable, but also as far isolated from nearby unwanted spin states as possible. For this purpose, a mainstream technique is to use laser-induced spin-dependent a.c. Stark shift [12, 38] that is nonlinear with respect to the magnetic quantum number, by which two-spin or three-spin manifolds have been isolated from other spin ground states [24, 28, 30, 32, 33]. However, currently the a.c. Stark shift technique is mostly based on relatively far-detuned lasers and can only realize rather weak nonlinearity with respect to the magnetic quantum number. Thus, it is often implemented at the cost of strongly shifting the spin states of interest, which causes noticeable scattering rates for these states and limits lifetime of the system to a 10-ms scale [24, 28, 30, 32, 33]. Very recently, a two-spin topological Fermi gas with long lifetime on the 100-ms scale has been achieved by removing unwanted spin ground states via near-resonant narrow-linewidth optical couplings [39]. It is of much interest to develop a general method for precisely engineering a few-spin manifold with an arbitrary number of spin ground states and long lifetime.

In this paper, we systematically study the performance of a highly nonlinear spin-discriminating (HNSD) method for realizing a highly isolated, highly stable manifold of an arbitrary number of spin states out of a larger number of spin ground states. Based on a combined magneto-optical approach, the unwanted spin ground states are strongly up-shifted, whereas a chosen number of spin states of interest remain almost unperturbed, which leads to a highly isolated and stable few-spin manifold. We realize this method using a Fermi gas of the alkaline-earth strontium (^{87}Sr) atoms and achieve a large nonlinearity parameter of 5500%, which demonstrates the HNSD nature of our method. Benefiting from the narrow-line intercombination transition of the AEAs, our method supports a long atomic lifetime on the 100-ms scale, which holds promise for significant future improvement with larger magnetic fields. We further verify the effective isolation of a two-spin system via two-photon Rabi oscillations. Our method provides a useful tool that is widely applicable for studying new types of topological quantum systems and many-body spin systems.

2 The method

Our method for realizing a highly isolated few-spin manifold builds on a combined magneto-optical approach: (i) magnetically separating the Zeeman energy levels of the spin excited states and (ii) removing unwanted spin ground states by spin-discriminating optical a.c. Stark shifts induced by near-resonant narrow-linewidth lasers. As illustrated in Fig. 1(a), under a sufficiently large magnetic field, the ground and excited spin states are Zeeman shifted such that the m_F-conserving π transition between ground and excited states has distinct resonance frequencies at different m_F values, with the adjacent resonance frequencies well separated by a spacing that is much larger than the characteristic transition linewidth. Thus, applying a laser beam that is near-resonance and blue-detuned with respect to one such π transition can strongly upshift the energy level of the corresponding $|m_F\rangle$ spin ground state and at the same time leave other spin ground states almost unperturbed (due to the much larger detunings). We note that AEAs provide an ideal platform for realizing this HNSD method because such atoms both have excited states that can be strongly Zeeman shifted under a realistic magnetic field, and have a narrow-linewidth intercombination transition. The insensitivity of AEA spin ground states to external fields provides one additional advantage that their energy level stability poses much less demanding requirements on the control precision of external magnetic fields.

3 Experimental setup and results

In the experiment, we use an ultracold Fermi gas of ^{87}Sr atoms, which have ten nuclear spin ground states and an intercombination transition ($\lambda_0 \approx 689.4$ nm, $\nu_0 \approx 434.8$ THz) with a narrow linewidth of $\Delta\nu_0 = 7.5$ kHz. Figure 1(b) shows the magnetic and optical key ingredients of

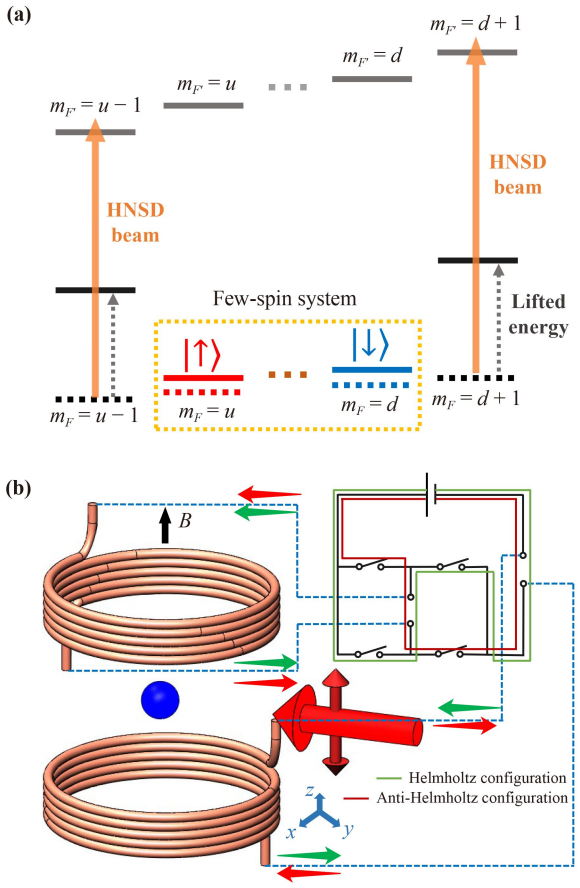

Fig. 1 The highly nonlinear spin-discriminating (HNSD) method for realizing an isolated few-spin system of a given number of spin states. **(a)** Diagram for the HNSD method. The spin ground states with $m_F = u$ to d form a $(d-u+1)$-spin manifold (yellow dashed rectangle) that remains almost unperturbed by an HNSD laser beam. By contrast, the nearby unwanted states of other m_F values are shifted far away from the aforementioned few-spin manifold by the near-resonance frequency component of the HNSD beam. Dashed (solid) horizontal lines denote the bare (shifted) ground-state energy levels without (with) the HNSD beam. **(b)** Magneto-optical setup for implementing the HNSD method. To generate a large homogeneous magnetic field using existing high-current coils, we implement an electrical H-bridge that can conveniently convert the anti-Helmholtz current configuration (used for magneto-optical trapping) into a Helmholtz configuration; see the illustrated circuit diagram. A 35-G magnetic field is applied at the atoms (blue ball) along the vertical (Z) direction, which defines the quantization axis for the atoms and induces a Zeeman energy splitting of about 13 MHz between adjacent magnetic levels $|m_{F'}\rangle$ for the $^3\mathrm{P}_1$ excited states (with $F' = \frac{11}{2}$). An HNSD laser beam (thick red arrow) of π polarization (thin arrow) passes through atoms along a horizontal direction.

the setup for implementing the HNSD method. To generate a sufficiently large homogeneous magnetic field in the vertical ($\hat{Z}$) direction, we build an electrical H-bridge that conveniently converts the anti-Helmholtz configuration (for magneto-optical trapping) of a pair of high-current coils into a Helmholtz configuration. Here, the electrical H-bridge consists of four high-power relays (Tyco Electronics, EV200AAANA). The switch from anti-Helmholtz to Helmholtz configuration is triggered by a transistor-transistor-logic (TTL) signal and finished in about 30 ms during the evaporative cooling stage. To protect the ultrahigh-vacuum science chamber from potential magnetization by large magnetic fields, we turn off the coil current well before the configuration switch, turn on the current again afterwards, and set an upper limit of 35 G for the field generated under the Helmholtz configuration in this work. At 35 G, adjacent $^3\mathrm{P}_1$ spin excited states are energetically separated by about 13 MHz (much larger than $\Delta\nu_0$), whereas the $^1\mathrm{S}_0$ spin ground states are barely separated (with kHz-scale spacing). Furthermore, at the end of evaporative cooling, we apply a vertically polarized HNSD laser beam onto the atoms to induce energy level shifts for selected unwanted $|m_F\rangle$ spin states based on m_F-conserving π transitions. This beam has about 200 μm $1/e^2$ radius and contains near-resonance frequency components for removing selected spin states.

In the remaining sections of this work, without loss of generality, we choose two spin ground states of interest as $|\uparrow\rangle \equiv {}^1\mathrm{S}_0|F=\frac{9}{2}, m_F=-\frac{9}{2}\rangle$ and $|\downarrow\rangle \equiv {}^1\mathrm{S}_0|F=\frac{9}{2}, m_F=-\frac{7}{2}\rangle$ to form an isolated two-spin manifold, and identify two nearby spin ground states $|m_F=-\frac{5}{2}\rangle$ and $|m_F=-\frac{3}{2}\rangle$ as the unwanted states. We note that removing these two unwanted states is sufficient for the isolation of the $|\uparrow\rangle$-and-$|\downarrow\rangle$ manifold when inter-spin couplings are restricted to two-photon Raman couplings, as is the case in this work.

3.1 Highly nonlinear spin-discriminating energy shifts

We experimentally demonstrate large differential a.c. Stark shift between selected spin states based on two-photon Raman spectroscopy. In the experimental sequence, an ultracold Fermi gas [40] is initially prepared in the $|\uparrow\rangle$ state, then energetically shifted by the HNSD beam under a magnetic field of 35 G, and finally coupled to the $|m_F=-\frac{5}{2}\rangle$ state via a two-photon Raman transition induced by two co-propagating, horizontally polarized Raman coupling beams. As the frequency difference Δf between two Raman beams varies, the transfer to $|m_F=-\frac{5}{2}\rangle$ is maximized when this frequency difference matches the energy level difference between $|m_F=-\frac{5}{2}\rangle$ and $|\uparrow\rangle$, and can be identified as a maximum loss of atomic population in $|\uparrow\rangle$. Figure 2(a) shows such population loss in $|\uparrow\rangle$ atoms under various values for the HNSD beam power, from which the energy difference between $|m_F=-\frac{5}{2}\rangle$ and $|\uparrow\rangle$ can be determined as the position of the on-resonance loss dip. A reference measurement is performed in the absence of the HNSD beam (namely under zero HNSD beam

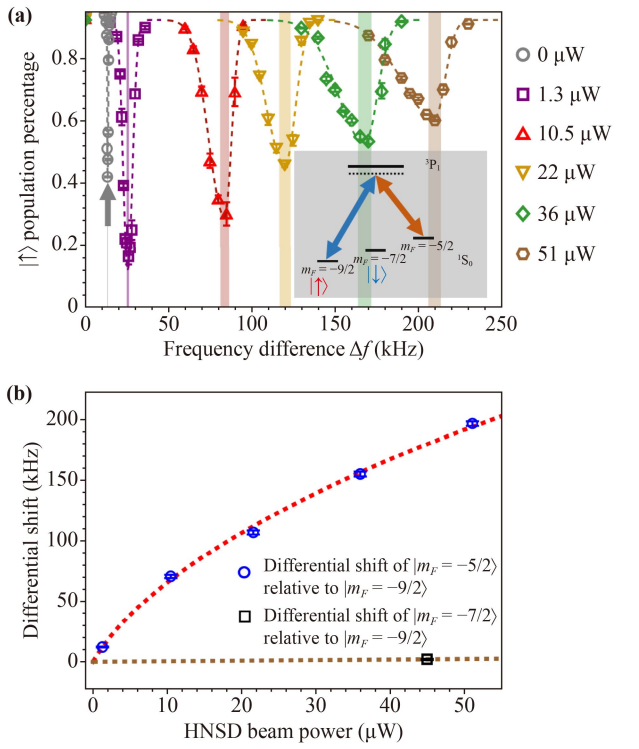

Fig. 2 Calibrating the light-induced differential energy shifts between spin ground states. **(a)** Population transfer from $|\uparrow\rangle$ to the $|m_F = -\frac{5}{2}\rangle$ state via a two-photon Raman transition. Atoms initially populated in the $|\uparrow\rangle$ state can be transferred to the $|-\frac{5}{2}\rangle$ state by absorbing a σ^+ photon and emitting a co-propagating σ^- photon with a different frequency. The energy difference between the $|-\frac{5}{2}\rangle$ and $|\uparrow\rangle$ states is determined as the frequency difference of the two Raman laser beams at the resonance of the two-photon transition, namely at the maximum population loss of the $|\uparrow\rangle$ state. Purple squares, red up-triangles, yellow down-triangles, green diamonds and brown hexagons are measurements under 1.3, 10.5, 22, 36 and 51 μW of HNSD beam power, respectively. Grey circles (with an arrow) denote a reference set of measurements without applying the HNSD beam. Dashed lines are asymmetric Gaussian fits for determining the position of maximum population loss of $|\uparrow\rangle$ (indicated by shaded areas). Inset: Illustration of the two-photon transition between $|\uparrow\rangle$ and $|-\frac{5}{2}\rangle$. **(b)** Laser-induced differential energy shifts as a function of the HNSD beam power. Blue circles show the measured energy shift (with the Zeeman splitting properly subtracted) of the $|-\frac{5}{2}\rangle$ state relative to $|\uparrow\rangle$. Black square shows a reference measurement for the energy shift of the $|\downarrow\rangle$ state relative to $|\uparrow\rangle$. Dashed lines are fittings based on Eq. (1).

power); see the grey open circles indicated by an arrow in Fig. 2(a). Subtracting the loss dip positions with and without the HNSD beam provides a determination of the HNSD laser-induced differential energy shift between the $|m_F = -\frac{5}{2}\rangle$ and $|\uparrow\rangle$ states. Here we emphasize that to make an energetically stable few-spin manifold, the unwanted nearby states should be up-shifted to avoid any potential decay mechanism. We experimentally implement such upward level shifting by choosing a blue frequency detuning for the corresponding HNSD frequency component with respect to the m_F-conserving π transition at $m_F = -\frac{5}{2}$.

The measured power dependence of the differential energy shift reveals the characteristic behavior of a two-level system with near-resonance coupling. By exact diagonalization of the Hamiltonian of a coupled two-level system [41–44], the general form of energy shift of the dressed ground state relative to the uncoupled "bare" ground state can be determined as

$$\delta_{\text{shift}} = \frac{\hbar}{2}\Delta\left(\sqrt{1+\frac{|\Omega|^2}{\Delta^2}}-1\right), \tag{1}$$

where $\hbar$ is the reduced Planck constant, Ω is the Rabi frequency, and Δ is the detuning of the laser frequency relative to the atomic resonance frequency of the bare two-level system. We note that δ_{shift} in Eq. (1) has a nonlinear dependence on $|\Omega|^2$ (or equivalently, the HNSD beam power) under relatively small values of Δ. Such nonlinear power dependence of the differential energy shift of the $|m_F = -\frac{5}{2}\rangle$ state relative to $|\uparrow\rangle$ is manifest in Fig. 2(b). Here, the blue circles denote measurements under a small blue detuning Δ with respect to the m_F-conserving π transition at $m_F = -\frac{5}{2}$, and the red dashed line is a fit based on Eq. (1), which yields a fitted detuning value of $\Delta \approx +100$ kHz. By contrast, due to much larger detunings (about +13 MHz and +26 MHz) with respect to the m_F-conserving π transitions at $m_F = -\frac{7}{2}$ and $-\frac{9}{2}$, the differential shift of the $|\downarrow\rangle$ state relative to $|\uparrow\rangle$ (black squares, brown dashed line) is two orders of magnitude smaller under similar HNSD beam power. Here we further define a nonlinearity parameter η_{nl} as

$$\eta_{\text{nl}} = \left| \frac{\delta_{\text{shift},-5/2} - \frac{\delta_{\text{shift},-7/2}+\delta_{\text{shift},-9/2}}{2}}{\frac{\delta_{\text{shift},-7/2}-\delta_{\text{shift},-9/2}}{\Delta m_2}\Delta m_1} - 1 \right|, \tag{2}$$

where the magnetic quantum number differences are given by $\Delta m_1 = -\frac{5}{2} - [(-\frac{7}{2}) + (-\frac{9}{2})]/2 = \frac{3}{2}$ and $\Delta m_2 = (-\frac{7}{2}) - (-\frac{9}{2}) = 1$. In the current HNSD setup for Fig. 2(b), we obtain $\eta_{\text{nl}} \approx 5500\%$, which realizes much larger nonlinearity than that in a conventional far-detuned a.c. Stark shift method (with $\eta'_{\text{nl}} \approx 17\%$ under large detunings of hundreds of MHz) [33], which thus supports naming our current method a "highly nonlinear spin-discriminating" method.

3.2 Lifetime

We study the atomic lifetime for $|\uparrow\rangle$ and $|\downarrow\rangle$ states under typical HNSD conditions based on experimental measurements and a theoretical model. The model is

mainly built on a master-equation approach similar to that in Ref. [45], which simplifies the optical Bloch equations [41–43, 46] via adiabatic elimination [45, 47]. This model, which is depicted by the following Eq. (3), takes into account two atomic loss mechanisms that simultaneously exist for a certain spin state: atomic loss due to the heating induced by optical scattering (the first term on the right-hand side), as well as spin depolarization caused by spontaneous emission (the second term on the right-hand side):

$$\frac{\mathrm{d}\rho_m}{\mathrm{d}t} = -\frac{\Omega_m^2}{4\Delta_m^2}\rho_m\Gamma_0\beta + \sum_{l\neq m}(1-\beta)\left(\frac{\Omega_l^2}{4\Delta_l^2}\rho_l\Gamma_{l,m} - \frac{\Omega_m^2}{4\Delta_m^2}\rho_m\Gamma_{m,l}\right). \tag{3}$$

Here for simplicity of presentation, Eq. (3) is written for a single frequency mode of the HNSD beam, where ρ_m is the atom number (in arbitrary unit) in the $|F,m\rangle$ spin ground state, t is the time, $\Gamma_0 = 2\pi\Delta\nu_0$, Ω_m and Δ_m are the Rabi frequency and detuning respectively for the m_F-conserving π transition $^1\mathrm{S}_0|F=\frac{9}{2},m\rangle \rightarrow {}^3\mathrm{P}_1|F'=\frac{11}{2},m\rangle$, and $\Gamma_{l,m}$ is the spontaneous decay rate from the spin excited state $^3\mathrm{P}_1|F',l\rangle$ to the spin ground state $^1\mathrm{S}_0|F,m\rangle$, which can be determined from Γ_0 and the related Clebsch–Gordan coefficients [42]. The parameter β is phenomenally introduced to denote the probability of atomic loss after scattering a single photon.

Scaling properties of characteristic time scales can be derived based on dimensional analysis for Eq. (3). We first note that the square of Rabi frequencies (Ω_m^2) is proportional to the HNSD laser beam power, and the detuning Δ_m is roughly given by the Zeeman splitting between corresponding spin excited states and is thus proportional to the magnetic field when the field is sufficiently large. Therefore, when the HNSD power increases by a factor of ξ, each Ω_m^2 increases by ξ, which makes the whole right-hand side of Eq. (3) enhanced by an overall factor of ξ. This corresponds to a reduction of characteristic lifetime by the factor of ξ, suggesting that the HNSD-setup-limited lifetime is inversely proportional to the HNSD power. On the other hand, when the magnetic field increases by ξ, each Δ_m increases by ξ, which makes the whole right-hand side of Eq. (3) reduced by an overall factor of ξ^2. This corresponds to an increase of the characteristic lifetime by a factor of ξ^2, suggesting that the HNSD-setup-limited lifetime is proportional to the square of the magnetic field.

A number of lifetime measurements are performed under a 35-G magnetic field using a two-frequency HNSD beam of 90 μW total power that induces more-than-100-kHz upward level shifts for the unwanted $|m_F=-\frac{5}{2}\rangle$ and $|m_F=-\frac{3}{2}\rangle$ states. Figure 3(a) shows sample measurements where initially atoms are almost equally distributed over $|\uparrow\rangle$ and $|\downarrow\rangle$, and then held for various amount of time under the HNSD setup. Evolution of the $|\uparrow\rangle$ ($|\downarrow\rangle$) atomic population is measured as a function of holding time, and an exponential decay fit is performed to determine the characteristic decay time. The parameter β is determined based on six groups of

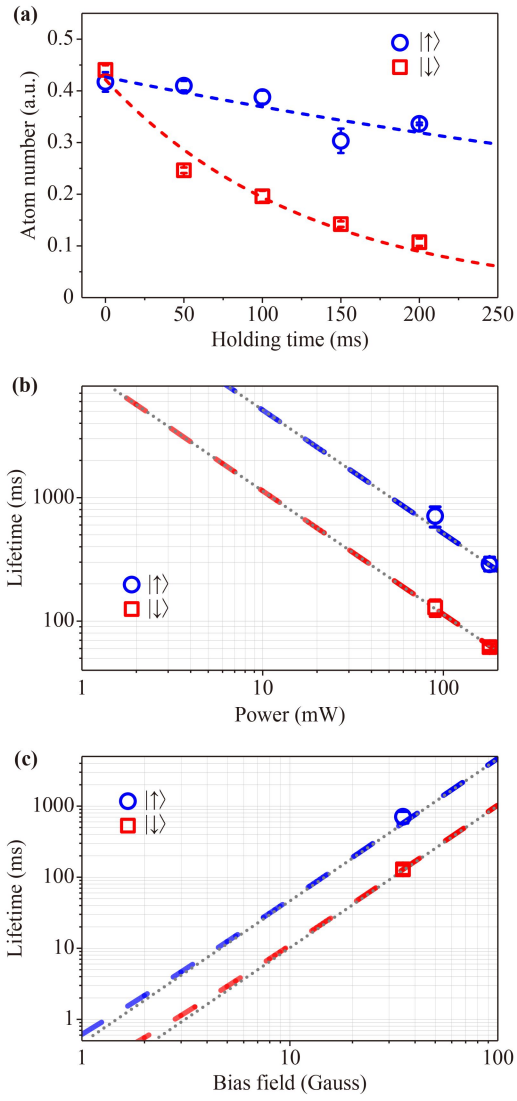

Fig. 3 Lifetime of spin states in an isolated two-spin manifold under the HNSD method. **(a)** Sample measurements for the evolution of atomic populations under various holding times in the presence of the HNSD beam, with atoms initially populated equally in the $|\uparrow\rangle$ and $|\downarrow\rangle$ states. Blue circle (red square) denotes the atomic population in $|\uparrow\rangle$ ($|\downarrow\rangle$), and dashed lines are exponential decay fits. **(b, c)** Lifetime for the spin configuration with atoms initially populated equally in the $|\uparrow\rangle$ and $|\downarrow\rangle$ states under different HNSD power (b) and magnetic field (c), respectively. Blue circles and red squares show lifetime measurements for $|\uparrow\rangle$ and $|\downarrow\rangle$. Blue and red thick dashed lines show lifetime simulations for $|\uparrow\rangle$ and $|\downarrow\rangle$, which only consider the atomic loss due to the HNSD setup. As reference, grey dotted lines show an inverse proportional relation in panel (b) or a quadratic relation in panel (c), with a slope of –1 or 2 in a log-log plot.

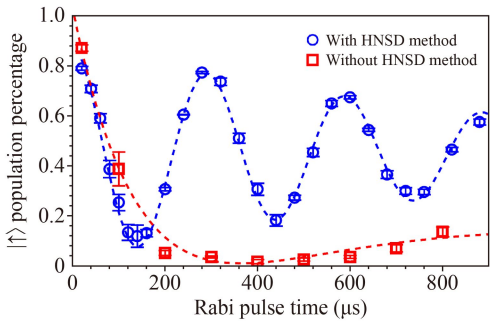

Fig. 4 Demonstration of an isolated two-spin system using two-photon Raman Rabi oscillation. Under a single Rabi pulse of on-resonance two-photon Raman coupling, evolution of the atomic population percentage in the $|\uparrow\rangle$ state is measured with the HNSD method implemented (blue circles) or without this implementation (red squares). Dashed lines are fits based on a damped oscillation model. With the HNSD method implemented, the measurements show a characteristic Rabi oscillation for the transition between states of a well-isolated two-spin system. By contrast, the measurements without implementing the HNSD method show no such characteristic oscillation. The comparison between these two measurements demonstrate the effectiveness of the HNSD method.

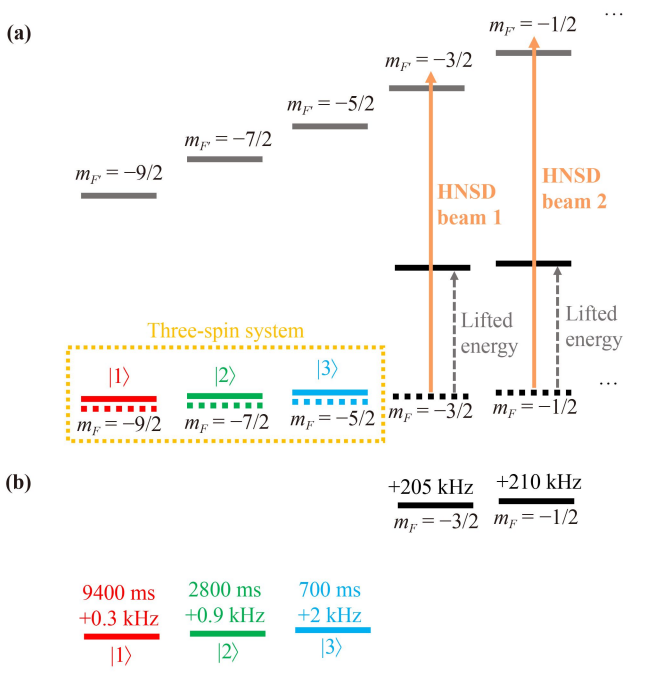

Fig. 5 The computed properties of a highly isolated, long-lived three-spin manifold generated by the HNSD method. **(a)** Schematic for generating a three-spin manifold. Here, the manifold consists of three spin ground states with $m_F = -\frac{9}{2}, -\frac{7}{2}, -\frac{5}{2}$. Two HNSD beams are applied to energetically up-shift the two adjacent unwanted spin states with $m_F = -\frac{3}{2}$ and $-\frac{1}{2}$. **(b)** Estimated energy shift and lifetime. Under a magnetic field of 100 G and 45 μW power in each HNSD beam that is blue detuned by 100 kHz with respect to the m_F-conserving π-transition at $m_F = -\frac{3}{2}$ or $-\frac{1}{2}$, the two unwanted spin states are up-shifted by more than 200 kHz, whereas the three spin states of interest are shifted by no more than a few kHz. Moreover, the three spin states of interest all have long lifetimes on the second scale (9.4 s, 2.8 s, 0.7 s). Here, the lifetime is computed for an initial spin configuration with all atoms polarized into the corresponding spin state. The computation only takes into account the effect of the HNSD setup.

lifetime data tested with different initial spin configurations or different HNSD beam power.

Our study reveals fairly long atomic lifetime under the typical HNSD setup. Figure 3(b) shows measured atomic lifetimes of (710 ± 130) ms and (130 ± 20) ms for $|\uparrow\rangle$ and $|\downarrow\rangle$ under a total HNSD power of 90 μW, a magnetic field of 35 G and an initial spin configuration where atoms are equally populated over $|\uparrow\rangle$ and $|\downarrow\rangle$. These lifetime results are significantly longer than the results in Ref. [33] based on a conventional far-detuned a.c. Stark shift approach. Under current experimental conditions, the lifetime is mainly limited by the heating induced by optical scattering with the HNSD beam. The HNSD-setup-induced heating rate is on the scale of 1000 nK/s, which is three orders of magnitude larger than the heating rate induced by the optical dipole trap. We also note that under our ultra-high vacuum condition (with the pressure below 1×10^{-11} Torr), the background collision rate is estimated to be less than $0.02\ \mathrm{s}^{-1}$, which is negligible for the current study.

The lifetime exhibits scaling properties similar to those suggested by the aforementioned dimensional analysis. The measurements and numerical simulations in Fig. 3(b) together show that the atomic lifetime indeed has an inverse proportional relation with the HNSD power. Furthermore, the simulations in Fig. 3(c) show that the atomic lifetime improves approximately quadratically with the magnetic field in the large-field regime. These scaling properties are useful for the further experimental improvement of the lifetime. We also monitor the small and slow escape of atoms from the $|\uparrow\rangle$-and-$|\downarrow\rangle$ manifold, and extract a long characteristic time of 3 seconds for the decay of the $|\uparrow\rangle$-and-$|\downarrow\rangle$ population fraction under the currently applied magnetic field.

3.3 Demonstration of a two-spin system using two-photon Raman Rabi oscillation

We further demonstrate a highly isolated two-spin system using two-photon Raman Rabi oscillation between the two spin states. Here, an ultracold Fermi gas is initially prepared in the $|\uparrow\rangle$ state. We then apply a HNSD beam that has two single-frequency components for moving away the $|m_F = -\frac{5}{2}\rangle$ and $|m_F = -\frac{3}{2}\rangle$ states. A pulse of two co-propagating Raman coupling beams passes through the atoms along the horizontal direction. These two beams have orthogonal polarizations in the

vertical and horizontal directions respectively, with their frequency difference matching the energy level difference between the $|\downarrow\rangle$ and $|\uparrow\rangle$ states. Atoms can thus be transferred from $|\uparrow\rangle$ to $|\downarrow\rangle$ via two-photon Raman processes. With a varying duration of the Raman pulse, evolution of the atomic population percentage in the $|\uparrow\rangle$ state shows a characteristic Rabi oscillation (Fig. 4, blue circles). By comparison, under on-resonance Raman Rabi pulse in the absence of HNSD beam, the $|\uparrow\rangle$ population percentage shows almost no Rabi oscillation. These two sets of measurements demonstrate the effectiveness of the HNSD method in creating a well isolated two-spin system.

3.4 Towards a manifold of an arbitray number of spin states

As an example, we now compute the properties of an experimentally realistic realization of a three-spin manifold; see Fig. 5. With a total HNSD power of $45 + 45 = 90$ μW and a magnetic field of 100 G, which is fairly feasible in future experiments, the two unwanted spin states (with $m_F = -\frac{3}{2}$ and $-\frac{1}{2}$) are up-shifted by a large amount of more than 200 kHz, whereas the spin states within the three-spin manifold are shifted by no more than a few kHz. Furthermore, the HNSD setup causes little heating effect to these three states of interest. When only the HNSD-setup-induced heating is considered, each of the three states has long lifetime on the second scale. Our HNSD approach is well applicable for generating a highly isolated, long-lived manifold of an arbitrary number of spin states.

4 Conclusion and discussion

In summary, we demonstrate an experimental method for achieving a highly isolated, least perturbed few-spin manifold of an arbitrary number of spin states. For systems with such few-spin manifolds, the HNSD method also allows for achieving long lifetime, which can be further significantly improved to the second scale or longer in systems where larger magnetic fields (hundreds of Gausses) can be safely applied, particularly in those systems with a UHV glass cell. Our method provides a prototypical example for utilizing the precision tool of narrow-linewidth ultrastable lasers to realize long-lived few-spin quantum gases, which will benefit the studies on topological spin systems such as Fermi gases with two- and higher-dimensional spin–orbit couplings.

Declarations The authors declare that they have no competing interests and there are no conflicts.

Availability of data and material The data that support the findings of this study are available from the corresponding author, upon reasonable request.

Acknowledgements We are grateful to Murray Barrett for very insightful discussions. We thank Meng Khoon Tey, Li-Yang Xie, Bo-Yang Wang, Yu-Dong Wei, Biao Wu, Shina Tan, Yige Lin, Xiaoji Zhou for discussion and technical support. This work was supported by the Chinese Academy of Sciences Strategic Priority Research Program under Grant No. XDB35020100, the National Key Research and Development Program of China under Grant No. 2018YFA0305601, the National Natural Science Foundation of China under Grant No. 11874073, the Hefei National Laboratory and the Scientific and Technological Innovation 2030 Key Program of Quantum Communication and Quantum Computing under Grant No. 2021ZD0301903. H.Z. and X.Z. conceived the project. W.-W.W., H.Z., C.Q., M.-C.L., R.W. performed the experiments. C.Q., H.Z., W.-W.W. performed the numerical computations. All authors contributed to the data analysis and the writing of this manuscript.

References

1. A. D. Ludlow, M. M. Boyd, J. Ye, E. Peik, and P. O. Schmidt, Optical atomic clocks, *Rev. Mod. Phys.* 87(2), 637 (2015)
2. C. Chin, R. Grimm, P. Julienne, and E. Tiesinga, Feshbach resonances in ultracold gases, *Rev. Mod. Phys.* 82(2), 1225 (2010)
3. P. Naidon and S. Endo, Efimov physics: A review, *Rep. Prog. Phys.* 80(5), 056001 (2017)
4. C. Monroe, W. C. Campbell, L. M. Duan, Z. X. Gong, A. V. Gorshkov, P. W. Hess, R. Islam, K. Kim, N. M. Linke, G. Pagano, P. Richerme, C. Senko, and N. Y. Yao, Programmable quantum simulations of spin systems with trapped ions, *Rev. Mod. Phys.* 93(2), 025001 (2021)
5. J. K. Asbóth, L. Oroszlány, and A. Pályi, A Short Course on Topological Insulators, Springer, 2016
6. X. L. Qi, Y. S. Wu, and S. C. Zhang, Topological quantization of the spin Hall effect in two-dimensional paramagnetic semiconductors, *Phys. Rev. B* 74(8), 085308 (2006)
7. X. J. Liu, K. T. Law, and T. K. Ng, Realization of 2D spin–orbit interaction and exotic topological orders in cold atoms, *Phys. Rev. Lett.* 112(8), 086401 (2014)
8. L. Huang, Z. Meng, P. Wang, P. Peng, S. L. Zhang, L. Chen, D. Li, Q. Zhou, and J. Zhang, Experimental realization of two-dimensional synthetic spin–orbit coupling in ultracold Fermi gases, *Nat. Phys.* 12(6), 540 (2016)
9. Z. Wu, L. Zhang, W. Sun, X. T. Xu, B. Z. Wang, S. C. Ji, Y. Deng, S. Chen, X. J. Liu, and J. W. Pan, Realization of two-dimensional spin–orbit coupling for Bose–Einstein condensates, *Science* 354(6308), 83 (2016)
10. W. Sun, B. Z. Wang, X. T. Xu, C. R. Yi, L. Zhang, Z. Wu, Y. Deng, X. J. Liu, S. Chen, and J. W. Pan, Highly controllable and robust 2D spin–orbit coupling for quantum gases, *Phys. Rev. Lett.* 121(15), 150401 (2018)
11. X. T. Xu, Z. Y. Wang, R. H. Jiao, C. R. Yi, W. Sun, and S. Chen, Ultra-low noise magnetic field for quantum gases, *Rev. Sci. Instrum.* 90(5), 054708 (2019)

12. J. Ye, H. J. Kimble, and H. Katori, Quantum state engineering and precision metrology using state-insensitive light traps, *Science* 320(5884), 1734 (2008)
13. A. V. Gorshkov, M. Hermele, V. Gurarie, C. Xu, P. S. Julienne, J. Ye, P. Zoller, E. Demler, M. D. Lukin, and A. M. Rey, Two-orbital $SU(N)$ magnetism with ultracold alkaline-earth atoms, *Nat. Phys.* 6(4), 289 (2010)
14. A. J. Daley, Quantum computing and quantum simulation with group-II atoms, *Quantum Inform. Process.* 10(6), 865 (2011)
15. S. Taie, R. Yamazaki, S. Sugawa, and Y. Takahashi, An $SU(6)$ Mott insulator of an atomic Fermi gas realized by large-spin Pomeranchuk cooling, *Nat. Phys.* 8(11), 825 (2012)
16. S. Stellmer, F. Schreck, and T. C. Killian, in: Annual Review of Cold Atoms and Molecules, Vol. 2, Chapter 1, 1st Ed., World Scientific, Singapore, 2014
17. G. Pagano, M. Mancini, G. Cappellini, P. Lombardi, F. Schafer, H. Hu, X. J. Liu, J. Catani, C. Sias, M. Inguscio, and L. Fallani, A one-dimensional liquid of fermions with tunable spin, *Nat. Phys.* 10(3), 198 (2014)
18. X. Zhang, M. Bishof, S. L. Bromley, C. V. Kraus, M. S. Safronova, P. Zoller, A. M. Rey, and J. Ye, Spectroscopic observation of $SU(N)$-symmetric interactions in Sr orbital magnetism, *Science* 345(6203), 1467 (2014)
19. F. Scazza, C. Hofrichter, M. Höfer, P. C. De Groot, I. Bloch, and S. Fölling, Observation of two-orbital spin-exchange interactions with ultracold $SU(N)$-symmetric fermions, *Nat. Phys.* 10(10), 779 (2014)
20. G. Cappellini, M. Mancini, G. Pagano, P. Lombardi, L. Livi, M. Siciliani de Cumis, P. Cancio, M. Pizzocaro, D. Calonico, F. Levi, C. Sias, J. Catani, M. Inguscio, and L. Fallani, Direct observation of coherent interorbital spin-exchange dynamics, *Phys. Rev. Lett.* 113(12), 120402 (2014)
21. Y. G. Lin, Q. Wang, Y. Li, F. Meng, B. K. Lin, E. J. Zang, Z. Sun, F. Fang, T. C. Li, and Z. J. Fang, First evaluation and frequency measurement of the strontium optical lattice clock at NIM, *Chin. Phys. Lett.* 32(9), 090601 (2015)
22. X. Tian, Q. Xu, M. Yin, D. Kong, Y. Wang, B. Lu, H. Liu, J. Ren, and H. Chang, Experiment study on optical lattice clock of strontium at NTSC, *Acta Opt. Sin.* 35(s1), s102001 (2015)
23. M. Mancini, G. Pagano, G. Cappellini, L. Livi, M. Rider, J. Catani, C. Sias, P. Zoller, M. Inguscio, M. Dalmonte, and L. Fallani, Observation of chiral edge states with neutral fermions in synthetic Hall ribbons, *Science* 349(6255), 1510 (2015)
24. B. Song, C. He, S. Zhang, E. Hajiyev, W. Huang, X. J. Liu, and G. B. Jo, Spin–orbit-coupled two-electron Fermi gases of ytterbium atoms, *Phys. Rev. A* 94, 061604(R) (2016)
25. L. F. Livi, G. Cappellini, M. Diem, L. Franchi, C. Clivati, M. Frittelli, F. Levi, D. Calonico, J. Catani, M. Inguscio, and L. Fallani, Synthetic dimensions and spin–orbit coupling with an optical clock transition, *Phys. Rev. Lett.* 117(22), 220401 (2016)
26. S. Kolkowitz, S. L. Bromley, T. Bothwell, M. L. Wall, G. E. Marti, A. P. Koller, X. Zhang, A. M. Rey, and J. Ye, Spin–orbit-coupled fermions in an optical lattice clock, *Nature* 542(7639), 66 (2017)
27. S. L. Campbell, R. B. Hutson, G. E. Marti, A. Goban, N. D. Oppong, R. L. McNally, L. Sonderhouse, J. M. Robinson, W. Zhang, B. J. Bloom, and J. Ye, A Fermi-degenerate three-dimensional optical lattice clock, *Science* 358(6359), 90 (2017)
28. B. Song, L. Zhang, C. He, T. F. J. Poon, E. Hajiyev, S. Zhang, X. J. Liu, and G. B. Jo, Observation of symmetry-protected topological band with ultracold fermions, *Sci. Adv.* 4(2), eaao4748 (2018)
29. A. Goban, R. B. Hutson, G. E. Marti, S. L. Campbell, M. A. Perlin, P. S. Julienne, J. P. D'Incao, A. M. Rey, and J. Ye, Emergence of multi-body interactions in a fermionic lattice clock, *Nature* 563(7731), 369 (2018)
30. B. Song, C. He, S. Niu, L. Zhang, Z. Ren, X. J. Liu, and G. B. Jo, Observation of nodal-line semimetal with ultracold fermions in an optical lattice, *Nat. Phys.* 15(9), 911 (2019)
31. L. Sonderhouse, C. Sanner, R. B. Hutson, A. Goban, T. Bilitewski, L. Yan, W. R. Milner, A. M. Rey, and J. Ye, Thermodynamics of a deeply degenerate $SU(N)$-symmetric Fermi gas, *Nat. Phys.* 16(12), 1216 (2020)
32. P. Lauria, W. T. Kuo, N. R. Cooper, and J. T. Barreiro, Experimental realization of a fermionic spin-momentum lattice, *Phys. Rev. Lett.* 128(24), 245301 (2022)
33. M. C. Liang, Y. D. Wei, L. Zhang, X. J. Wang, H. Zhang, W. W. Wang, W. Qi, X. J. Liu, and X. Zhang, Realization of Qi–Wu–Zhang model in spin–orbit-coupled ultracold fermions, *Phys. Rev. Res.* 5(1), L012006 (2023)
34. J. Dalibard, F. Gerbier, G. Juzeliunas, and P. Ohberg, Colloquium: Artificial gauge potentials for neutral atoms, *Rev. Mod. Phys.* 83(4), 1523 (2011)
35. N. Goldman, G. Juzeliunas, P. Ohberg, and I. B. Spielman, Light-induced gauge fields for ultracold atoms, *Rep. Prog. Phys.* 77(12), 126401 (2014)
36. H. Zhai, Degenerate quantum gases with spin–orbit coupling: A review, *Rep. Prog. Phys.* 78(2), 026001 (2015)
37. L. Zhang and X. J. Liu, in: Synthetic Spin–Orbit Coupling in Cold Atoms, Chapter 1, pp 1–87, edited by W. Zhang, W. Yi, and C. A. R. S. de Melo, World Scientific, Singapore, 2018
38. G. W. F. Drake (Ed.), Atomic, Molecular, & Optical Physics Handbook, American Institute of Physics, Woodbury, N.Y., 1996
39. H. Zhang, W. -W. Wang, C. Qiao, L. Zhang, M. -C. Liang, R. Wu, X. -J. Wang, X. -J. Liu, and X. Zhang, Topological spin–orbit-coupled fermions beyond rotating wave approximation, under review by *Phys. Rev. Lett.*
40. W. Qi, M. C. Liang, H. Zhang, Y. D. Wei, W. W. Wang, X. J. Wang, and X. Zhang, Experimental realization of degenerate Fermi gases of ^{87}Sr atoms with 10 or two spin components, *Chin. Phys. Lett.* 36(9), 093701 (2019)
41. H. J. Metcalf and P. Straten, Laser Cooling and Trapping, Springer, New York, USA, 1999
42. C. J. Foot, Atomic Physics, Oxford: Oxford University Press, 2005
43. D. A. Steck, Quantum and Atom Optics, available online at URL: steck.us/teaching, revision 0.12. 5, 26 January 2019

44. H. Zhai, Ultracold Atomic Physics, Cambridge University Press, Cambridge, 2021
45. C. Qiao and W. Zhang, Spontaneous decay-induced quantum dynamics in Rydberg-blockaded Λ-type atoms, *J. Phys. At. Mol. Opt. Phys.* 54(20), 205501 (2021)
46. C. Cohen-Tannoudji and D. Guery-Odelin, Advances in Atomic Physics: An Overview, Singapore: World Scientific, 2011
47. M. O. Scully and M. S. Zubairy, Quantum Optics, Cambridge University Press, Cambridge, 1997